PROTEIN STABILIZED Au NANOCLUSTERS: SPECTRAL PROPERTIES AND PHOTOSTABILITY

V. Poderys [a], **M. Matulionytė-Safinė** [a, b], **D. Rupšys** [b], **and R. Rotomskis** [a, b]

[a] *Biomedical Physics Laboratory, National Cancer Institute, P. Baublio 3b, LT-08406 Vilnius, Lithuania*
[b] *Biophotonics Group of Laser Research Centre, Vilnius University, Saulėtekio 9, LT-10222 Vilnius, Lithuania*
E-mail: ricardas.rotomskis@nvi.lt

Bovine serum albumin stabilized gold nanoclusters (BSA-Au nanoclusters) have been widely studied due to their possible applications in biomedicine as sensors, fluorescent or multi-modality markers, and therapeutic agents. Synthesis and optical properties of these nanoclusters have been extensively investigated; however, there is still very little data on photostability of BSA-Au nanoclusters. Photostability of BSA-Au nanoclusters is of major importance for a variety of applications, such as material sensing and fluorescence imaging. Herein we demonstrate that after synthesis the BSA-Au solution has two photoluminescence (PL) bands peaking at 468 and 660 nm. Nevertheless, a different behaviour of the PL bands at 468 and 660 nm upon irradiation indicates that only band at 660 nm is related to PL of Au nanoclusters. BSA-Au nanoclusters exhibit great colloidal stability and do not undergo irreversible changes when heated up to 65 °C. However, irradiation of BSA-Au nanoclusters causes a wavelength dependent decrease of intensity and a hypsochromic shift of the PL band at 660 nm which is proportional to the delivered dose. The shift of the PL band at 660 nm could occur due to loss of several gold atoms in Au nanoclusters and/or due to deterioration of a nanoparticle coating layer. We have also demonstrated that the photostability of BSA-Au nanoclusters increases in the cell growth medium.

Keywords: photoluminescent gold nanoclusters, bovine serum albumin, spectral properties, stability, irradiation, atomic force microscopy

PACS: 78.67.Bf

1. Introduction

New properties emerge when the size of matter is reduced from the bulk to the nanometre scale. These new properties, including optical, magnetic, electronic, and structural ones, make nanosized particles (generally 1–100 nm in diameter) very promising for a wide range of biomedical applications such as cellular imaging, molecular diagnostics and targeted therapy. Gold nanoparticles have been brought to the forefront of cancer research in recent years because of their facile synthesis and surface modification, tuneable optical properties as well as excellent biocompatibility. Gold nanoclusters (Au NCs) are assemblies of a small number (2–30) of gold atoms, typically no bigger than 1–2 nm in diameter. Such metal nanoclusters, composed of only several tens of atoms, exhibit molecule-like electronic transitions as the density of states is insufficient to merge the valence and conduction bands [1, 2]. At sizes comparable to the Fermi wavelength of an electron (~0.7 nm in the case of gold), optical properties are significantly modified and discrete nanocluster energy levels become accessible [3].

To prevent nanoclusters from aggregation in aqueous solutions they are coated with stabilizing agents. A lot of different materials can be used as stabilizing agents, but in order to use nanoclusters in biological applications, the surface coating should be biocompatible. A few years ago there were the first attempts to use proteins (bovine serum albumin, BSA) as stabilizing agents [4–6]. Reduced gold atoms aggregate within the BSA molecule forming a gold nanocluster. This protein directed synthesis of highly fluorescent gold nanoclusters was firstly introduced by Xie et al. [4].

Currently, considerable research efforts are directed towards investigation of Au NCs synthesis [4–10], structure [7, 11, 12], optical properties [4, 13–16], photostability [17–21] and possible applications for material sensing [5, 22–24] as fluorescence [25, 26] and dual-modality imaging contrast agents [27, 28]. However, colloidal stability, photostability, dependence of optical

properties on temperature, interaction of BSA-Au NCs with biomolecules are still poorly investigated.

In this study, BSA-Au NCs optical properties, PL dependence on temperature, colloidal stability and photostability in aqueous and biological medium were investigated.

2. Materials and methods

2.1. Chemicals

BSA (V fraction, $M \sim 66$ kDa), $HAuCl_4 \times$ aqua (~52% Au basis, $M = 339.79$ kDa) and NaOH were purchased from *Sigma-Aldrich* (Germany) and used without further purification. Deionised water was produced using the ultrapure water system MicroPure UV (*TKA*, Germany).

2.2. Synthesis of BSA-Au nanoclusters

The BSA-Au nanoclusters (BSA-Au NCs) were synthesized according to the previously reported procedure [4] with slight modifications. Typically, an aqueous $HAuCl_4$ solution (5 mL, 37 °C, $c = 5.27 \times 10^{-3}$ M) was added to a BSA solution (5 mL, 37 °C, $c = 7.53 \times 10^{-4}$ M) under vigorous stirring. A NaOH solution (0.5 mL, 1.0 M) was introduced 2 min later, and the reaction was allowed to proceed under vigorous stirring for 12 h at a temperature of 37 °C. We tried to use various BSA:Au molar ratios (1:2; 1:5; 1:7; 1:13; 1:25; 1:35) for the BSA-Au NCs synthesis; however, the most intense PL was observed using the abovementioned synthesis procedure (BSA:Au molar ratio 1:7) (Fig. 1). All further experiments were performed using this BSA-Au NCs solution.
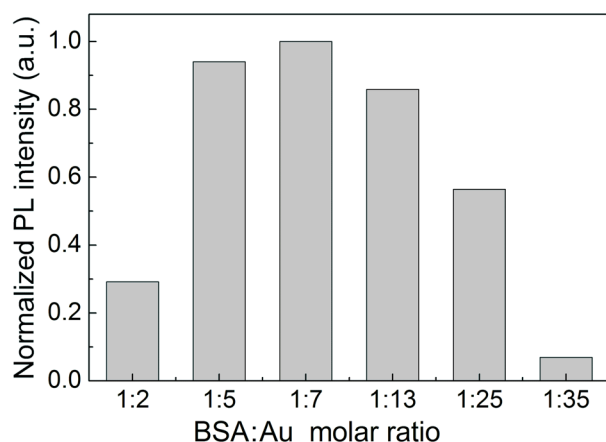

Fig. 1. The normalized PL intensity of synthesized BSA-Au NCs using different BSA:Au molar ratios.

2.3. Spectroscopic measurements

The steady state absorption and PL spectra of Au-BSA NCs were measured using a UV-visible absorption spectrometer Varian Carry 50 (*Varian Inc.*, Australia) and a fluorescence spectrometer Varian Cary Eclipse (*Varian Inc.*, Australia).

HellmaOptik (*Jena*, Germany) quartz cells (optical path length 1 cm) were used for all optical measurements.

2.4. Photostability measurements

The photostability of BSA-Au NCs was measured by irradiating 2 ml of the sample solution in quartz cells (exposed area was 1 cm^2) with a Xenon light source Max-301 (*Asahi Spectra Inc.*, Japan) ($\lambda = 280$ nm, FWHM = 32 nm, $I = 7$ mW/cm^2; $\lambda = 492$ nm, FWHM = 14 nm, $I = 24$ mW/cm^2) or a continuous wave diode laser ($\lambda = 405$ nm, $I = 50$ mW/cm^2). The irradiation procedure was carried out until the BSA-Au NCs PL intensity decreased by more than 70%. During the irradiation, the solutions were stirred using a magnetic stirrer.

2.5. Measurements of spatial characteristics

The hydrodynamic diameter was measured using a dynamic light scattering device Zeta Plus PALS (*Brookhaven Inc.*, USA). BSA-Au NCs samples for atomic force microscopy (AFM) imaging were prepared by casting a drop (20 μL) on a freshly cleaved mica surface spinning at 1000 rpm (spin coating). An atomic force microscope Innova (*Veeco Inc.*, USA) was used for BSA-Au NCs imaging in the tapping mode using silicon nitride probes MPP12283 (*Veeco Inc.*, USA).

3. Results

3.1. Spectral characteristics of BSA-Au nanoclusters

The absorption, PL and PL excitation spectra of the freshly synthesized BSA-Au nanoclusters are presented in Fig. 2. The absorption of Au-BSA NCs increases in a short wavelength region and has an absorption band with a maximum around 278 nm, the same region where pure BSA has an absorption peak (Fig. 2). The PL spectrum of the BSA-Au NCs solution has two bands in the visible region. The peak positions of these bands are at 468 and 660 nm. The components used for BSA-Au NCs synthesis ($HAuCl_4$, BSA) or a mixture of those two materials do not have any PL band in the red spectral

region (600–700 nm) (data not shown). $HAuCl_4$ does not fluoresce at all. BSA has a PL band around 338 nm (λ_{ex} = 280 nm), however, pure BSA also exhibits weak fluorescence in the blue region at 468 nm (λ_{ex} = 405 nm) (data not shown). The PL excitation spectrum of the BSA-Au NCs solution (λ_{em} = 660 nm) has a band at 500 nm and a gradual slope to the longer wavelength region. The PL excitation spectrum does not coincide with the absorption spectrum of BSA-Au NCs. Only a slight shoulder of the absorption spectrum around 500 nm was detected.

Optical properties of the BSA-Au NCs solution (absorption, PL intensity, PL band position and width) remained stable for more than one month (solution was kept at 4 °C, in the dark) (Fig. 3(a)). Our results show that the solution of BSA-Au NCs is stable and does not degrade for more than one month when kept in the dark at 4 °C.

3.2. The effect of temperature increase on the optical properties of BSA-Au nanoclusters

The influence of temperature increase on the BSA-Au NCs PL is presented in Fig. 3(b). The increase of the solution temperature from 5 to 65 °C caused the decrease of BSA-Au NCs PL intensity (by 77%), the bathochromic shift of the PL band by 23 nm (from 660 to 683 nm), and the increase of the PL band width (from 90 to 107 nm). As the temperature increased from 5 to 37 °C reaching the "biological" temperature, the PL intensity decreased twice. The absorption spectrum of BSA-Au NCs did not change during the heating–cooling cycle (data not shown). After cooling down the BSA-Au NCs solution to room temperature, all characteristics of the PL band returned to the ones observed before the heating (Fig. 3(b)).

3.3. The size of BSA-Au nanoclusters

The hydrodynamic particle size distributions of BSA and Au-BSA NCs solutions are presented in Fig. 4(a). The hydrodynamic size of BSA molecules varies from 6 to 8.3 nm (peak of size distribution is at
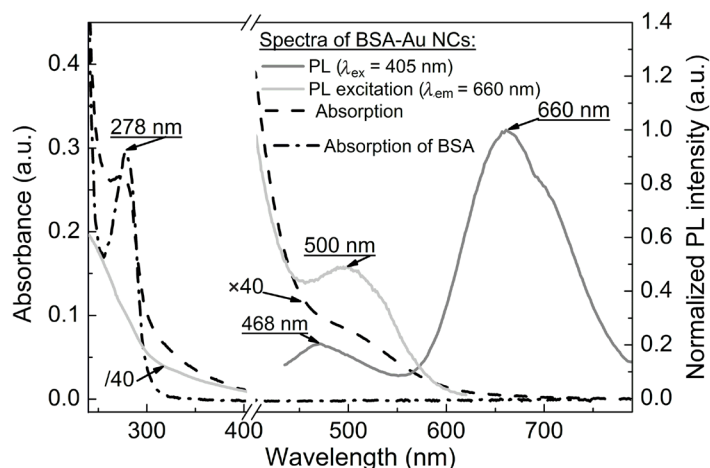

Fig. 2. Absorption (black dashed line), PL excitation (λ_{em} = 660 nm, light grey line), PL emission (λ_{ex} = 405 nm, dark grey line) spectra of BSA-Au NCs, and the BSA absorption spectrum (black dash-dotted line).
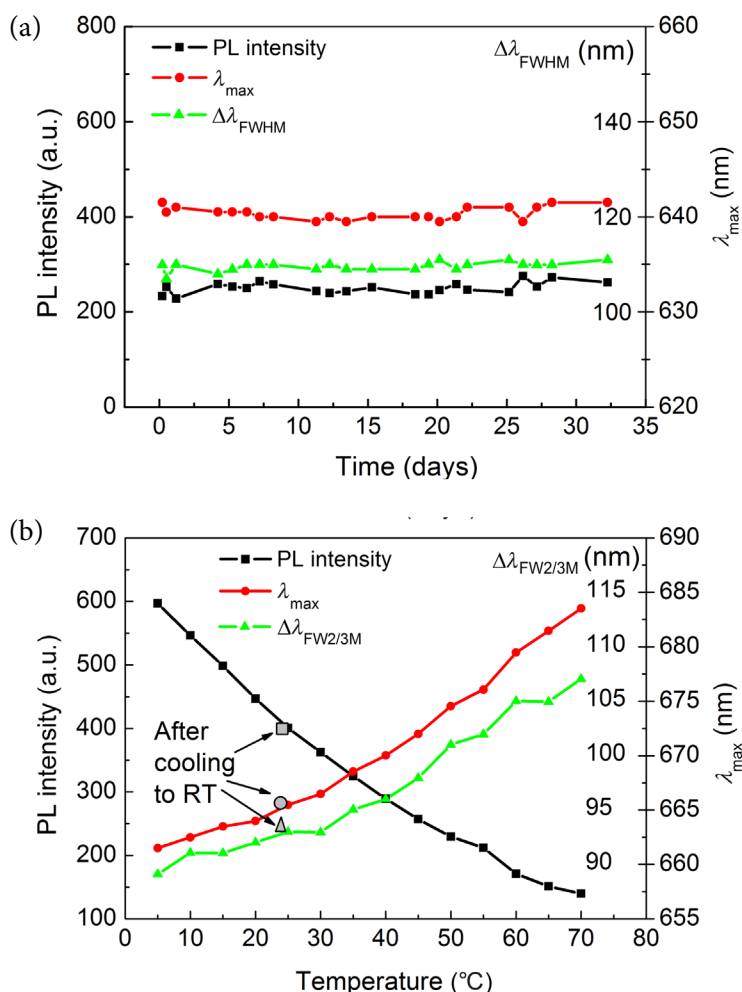

Fig. 3. Dependence of BSA-Au NCs PL spectral properties on storing time (a) and on temperature (b) (c (BSA-Au NCs) = 1.5 × 10⁻⁴ M, λ_{ex} = 405 nm).

6.9 nm) while the size of BSA-Au NCs appeared to be bigger: from 8 to 11 nm (peak of size distribution is at 9.4 nm) in diameter in comparison with BSA.

The AFM images of BSA and BSA-Au NCs are presented in Fig. 4(b, c). In both cases disc shape structures are seen on the mica surface. There is no detectable difference in the diameter of these structures (in both cases ~30 nm). However, the height of BSA-Au NCs is slightly bigger (~1.3 nm) than that of BSA (~0.9 nm) (Fig. 4).

3.4. Photostability of BSA-Au nanoclusters

Irradiating BSA-Au NCs solutions with 280, 405 and 492 nm wavelength light induced different changes in the PL spectra (Fig. 5). 492 nm light had no effect on the spectroscopic characteristics of the PL band at 468 nm; however, PL intensity at 660 nm decreased and underwent a continuous hypsochromic PL band maximum shift (Fig. 5), which was dependent on the delivered dose.

The irradiation of the BSA-Au NCs sample with 405 nm wavelength light caused the decrease of the PL intensity of both PL bands (at 468 and 660 nm) and a hypsochromic shift of the emission band at 660 nm to a shorter wavelength region. Exposure to 280 nm light led to the decrease of PL intensity and a hypsochromic shift of the PL band at 660 nm. The effect on the PL band at 468 nm was completely different: PL intensity of this band increased more than 5 times and the band shifted to the shorter wavelength region.

The irradiation caused big and irradiation-wavelength dependant changes in the BSA-Au NCs PL spectra. However, changes in the BSA-Au NCs absorption spectra were very small and similar in all three cases:

a slight increase of absorbance in the blue spectral region (data not shown).

Changes of the PL band at 660 nm were similar under irradiation with 280, 405 and 492 nm light: the PL intensity decreased and the band shifted to the shorter wavelength region. However, the PL intensity decrease rate was higher when a shorter wavelength was used for irradiation (Fig. 6). The observed PL band shift to the shorter wavelength was also bigger when the shorter wavelength light was used.

The photostability of BSA-Au NCs in the Opti-MEM cell growth medium was also investigated (Fig. 6). The BSA-Au NCs exhibit greater photostability in the cell growth medium Opti-MEM than in water.

4. Discussion

High PL quantum yield is one of the fundamental characteristics for the fluorescent probes, therefore, we tried various BSA:Au molar ratios (1:2; 1:5; 1:7; 1:13; 1:25; 1:35) for BSA-Au NCs synthesis. The BSA-Au NCs exhibited the most intense PL when the BSA:Au molar ratio 1:7 was used (Fig. 1).

The size of nanoparticles is essential for the pharmacokinetics, biodistribution and renal clearance *in vivo* [18]. Hydrodynamic size distribution data show that BSA-Au NCs are quite homogeneous, with a diameter around 9.5 nm that is about 2.5 nm larger in comparison with the hydrodynamic diameter of pure BSA (Fig. 4(a)). In literature it is reported that a gold nanocluster composed of 25 atoms is less than 1 nm in diameter [22, 29]. Formation of such nanoparticle in a protein template or attached to protein should not cause increase in the BSA size by 2.5 nm. This indicates that the size increase after synthesis could be due
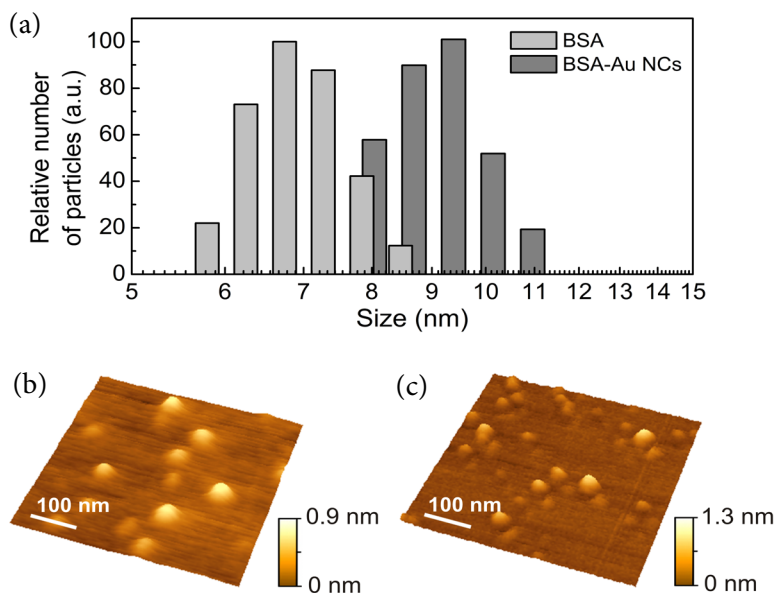

(a)

(b)

(c)

Fig. 4. Hydrodynamic size distribution of BSA-Au NCs and BSA measured using the dynamic light scattering technique (a) and topography of BSA (b) and BSA-Au NCs (c) spread on the mica surface measured using an atomic force microscope.
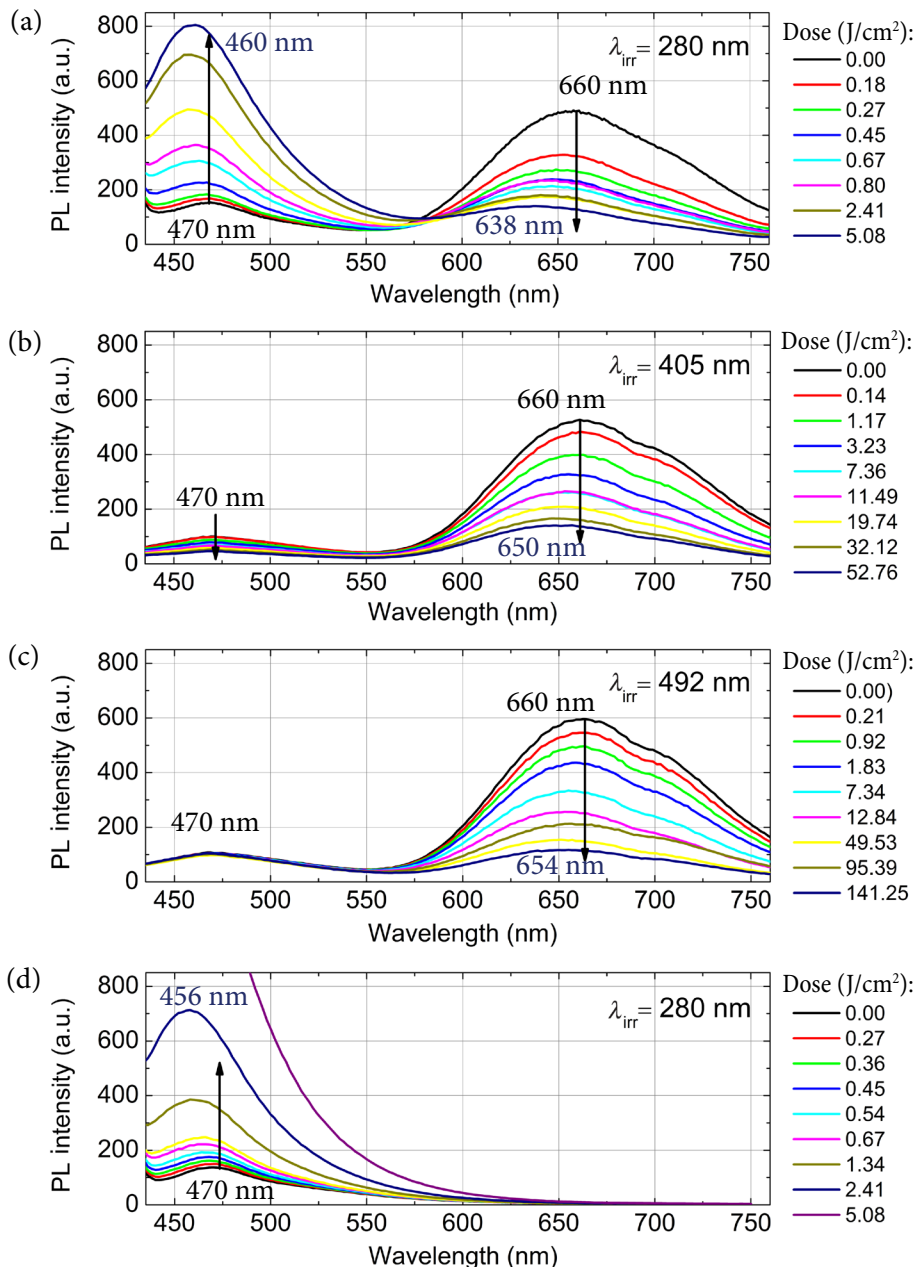
Fig. 5. PL spectra of the BSA-Au NCs in aqueous solutions after irradiation with 280 nm (a), 405 nm (b), 492 nm (c) light and the PL spectrum of BSA after irradiation with 280 nm light (d). PL emission spectra were obtained under the excitation at 405 nm. Arrows indicate spectral changes as the irradiation dose increases.

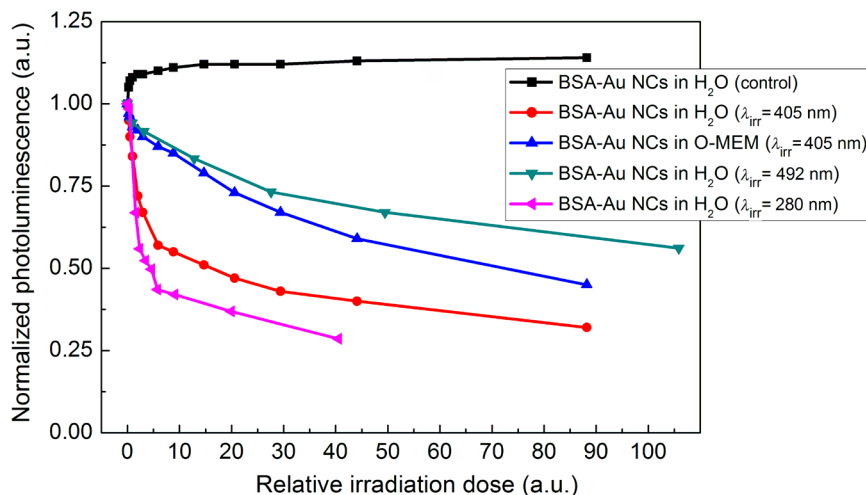Fig. 6. Dependence of the normalized PL intensity of BSA-Au NCs at 660 nm on a relative irradiation dose (λ_{ex} = 405 nm). The relative irradiation dose refers to a dose divided by the absorbance of BSA-Au NCs at the wavelength used for irradiation.

to the transformation of the secondary structure of BSA induced by formation of a gold nanocluster inside the protein [30].

The absorption spectra of pure BSA and BSA-Au NCs have a band around 278 nm (Fig. 2) that is caused by the absorption of constituent aromatic amino acids of BSA. However, this band is not present in the PL excitation spectrum of BSA-Au NCs. This indicates that there is no Förster resonance energy transfer (FRET) from tryptophan to a gold nanocluster or this process is very weak. However, some authors claim that FRET from tryptophan to Au NCs reaches up to 55% [32]. Raut et al. calculated the FRET efficiency by comparing the fluorescence (FL) lifetime of tryptophan in BSA and in BSA-Au NCs. Nevertheless, it was reported that in the case of BSA-Au NCs the FL band of tryptophan is blue shifted by 10–20 nm compared to the FL band of tryptophan in native BSA [32, 33]. It is known that tryptophan FL is highly sensitive to the environment and this leads to changes in FL intensity, FL band position and FL lifetime [34]. Therefore FL decay change could be related not to FRET but to conformational changes of BSA.

AFM measurements show that BSA dispersed on the mica surface loses its prolate ellipsoid structure with dimensions of 14 × 4 × 4 nm [35] and flattens (Fig. 4(b)). Similar results are obtained in the case of BSA-Au NCs (Fig. 4(c)). In both cases disc shape objects are observed on the mica surface, however, the height of BSA-Au NCs is slightly bigger. Interactions and bonds of the side chains of amino acids that form the backbone of protein determine its tertiary structure. Change of the surrounding medium and interaction with the mica surface can cause changes in the BSA structure. The radius of BSA-Au NCs in a solution measured with a dynamic light scattering method (this method approximates the shape of particles as spheres) was 4.7 nm (Fig. 4(a)). The volume of an ellipsoid can be calculated using the equation

$$V = \frac{4}{3} \cdot \pi \cdot a \cdot b \cdot c , \qquad (1)$$

where a, b and c are the radiuses of an ellipsoid (in the case of the sphere $a = b = c$).

If we assume that during the flattening process the volume of BSA-Au NC does not change, then

the compression of the sphere ($a = b = c = 4.7$ nm) to an oblate ellipsoid of 1.3 nm in height ($a = b$, $c = 0.65$ nm) leads to the formation of a similar structure as observed with AFM (Fig. 7). The diameter of the oblate ellipsoid produced by compressing the sphere (9.4 nm in diameter) is ~26 nm. The results calculated using this model are in good agreement with our experimental data. BSA-Au NCs dispersed on the mica surface are slightly bigger in diameter by approximately 4 nm. This can be caused by the AFM "tip imaging effect". Due to the "tip imaging" the measured width of the objects is always slightly increased, therefore differences in the diameter of pure BSA and BSA-Au NCs were not so noticeable.

The height of the BSA-Au NCs spread on the mica surface is only 1.3 nm, therefore it is possible to conclude that the size of a gold cluster embedded into BSA should not be bigger than 1.3 nm in diameter, because it is difficult to assume that the gold cluster can be squeezed or deformed on the mica surface.

It is well known that the PL emission wavelength of a gold nanocluster depends on the size and can be evaluated using a simple equation [36]

$$N = \left(\frac{e \lambda_{max} E_F}{hc} \right)^3 , \qquad (2)$$

where N is the number of gold atoms per cluster, λ_{max} is the wavelength at the emission band maximum, E_F is the Fermi energy of bulk gold in eV (5.53 eV), e is the number equal to electron charge, h is the Planck constant and c is the speed of light. According to this equation, the synthesized BSA-Au NC ($\lambda_{max} = 660$ nm) is composed of 29 gold atoms. Results of our experimental investigations show that the Au NC embedded into the BSA template is not bigger than 1.3 nm and contains less than 29 Au atoms.

In literature it was reported that BSA-Au NCs fluoresce in the red spectral region [4, 14–16, 30, 37] and the PL band at 640–700 nm corresponds to the PL of Au NCs that are formed inside BSA. Some papers reported that during synthesis two types of photoluminescent BSA-Au NCs are formed: blue photoluminescent NCs (PL λ_{max} ~ 470 nm) and red photoluminescent NCs (PL λ_{max} ~ 660 nm) [4, 30, 38]. However, it should be noted that these authors used ascorbic acid as a reducing agent. The papers that reported synthesis using NaOH as a reducing agent [13, 39]
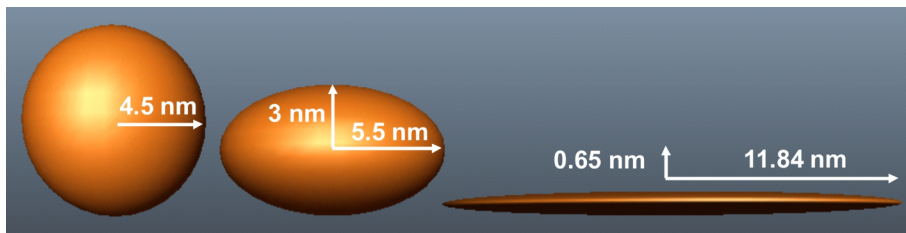

Fig. 7. A theoretical model shows how BSA-Au NC flattens spread on the mica surface in comparison to a spherical shape in a solution.

attribute a PL band around 470 nm to the PL of protein. Moreover, using mass spectroscopy Das et al. demonstrated that performing the synthesis of BSA-Au NCs using NaOH as a reducing agent, only Au_{25} nanoclusters were formed [40]. Both Au_8 and Au_{25} nanoclusters were formed when a different reducing agent (ascorbic acid) was used. Our results have shown that the aqueous solution of pure BSA also exhibits a weak fluorescence in the blue region (λ_{ex} = 405 nm) (data not shown), which proves that the PL band at 470 nm in the PL spectrum of BSA-Au NCs corresponds to the fluorescence of BSA.

The BSA-Au NCs PL dependence on the temperature is presented in Fig. 3(b). Heating of the BSA-Au NCs solution led to the decrease of BSA-Au NCs PL intensity. Simultaneously, a hypsochromic shift of the PL band of BSA-Au NCs was observed. Zhang et al. reported that conformational changes of a BSA ligand in BSA-Au NCs occur at ~58 °C, however, our results have shown that the PL changes of BSA-Au NCs during the heating–cooling cycle are reversible, moreover, heating from 5 to 65 °C does not affect absorption of BSA-Au NCs. It is known that heat-treated serum albumin undergoes two structural changes; the first stage is reversible whilst the second stage is irreversible but does not necessarily results in a complete destruction of the ordered structure [41–43]. Heating the BSA up to 65 °C can be regarded as staying in the first BSA structural stage, and subsequent heating above 65 °C as reaching the second stage. After the synthesis, BSA changes the conformation [30]. Recently Chib et al. [33] has shown that BSA Au nanoclusters are more robust to changes in their environment than BSA (including increase of temperature). Their results impose that in this temperature interval BSA-Au NCs should be more stable than BSA and should not undergo irreversible changes.

Our results confirm that BSA-Au NCs are not damaged during heating, therefore, the decrease of BSA-Au NCs PL intensity is probably caused by the decrease of the BSA-Au NCs PL quantum yield. These reversible changes of the emission intensity or the shift of emission maxima with temperature could be used for temperature measurements of the BSA-Au NCs surroundings.

The investigation of BSA-Au NCs photostability showed that the photostability depends on the wavelength of light used for irradiation (Fig. 5). Irradiation with 280 nm light causes an increase in the emission intensity at 468 nm and a decrease at 660 nm. Independent of the irradiation wavelength PL intensity at 660 nm decreased and the maximum is shifted to the shorter wavelength region. There are several possible causes that could explain the decrease of the BSA-Au NCs PL intensity at 660 nm. The first one is the photodegradation of nanoclusters. Irradiation of the BSA-Au NCs sample with 405 and 492 nm wavelength light caused a hypsochromic shift of the emission band from 660 to 652 nm. According to the calculations based on Eq. 2, the hypsochromic shift of the fluorescence band by 8 nm could reflect loss of one gold atom in a cluster.

Irradiation with 280 nm light causes a larger hypsochromic shift (22 nm). Such a shift could be caused by loss of 3–4 gold atoms in Au NCs. It is known that Au NCs composed of a specific number of gold atoms show high stability. These numbers are called "magic numbers". The closest magic number to 29 is 25. Therefore, it is likely that during irradiation Au NCs degrade and more stable Au NCs composed of 25 atoms are formed, which causes a hypsochromic shift of the PL band.

Another possible explanation for the PL intensity decrease and hypsochromic shift would be the deterioration of a nanoparticle coating layer. It was shown that the enzymatically generated H_2O_2 and enzymatic proteolysis induces degradation of BSA-Au NCs corona and causes a hypsochromic shift and the decrease of PL intensity [22, 23].

The degradation of a nanoparticle coating usually leads to a decrease in PL intensity [17, 45]. These two processes (nanocluster deterioration and coating degradation) can take place simultaneously and result in a hypsochromic shift of the PL band and intensity decrease under irradiation. Fluorescence of BSA can be excited only by irradiation at 280 nm. Irradiating the samples with 492 nm excites only Au NCs. It seems that in this case direct photodegradation of BSA is impossible. However, Au NCs can generate free radicals [46, 47] or singlet oxygen [48]. This can lead to degradation of BSA. Irradiation of BSA-Au NCs at 280 nm leads to a much faster PL intensity decrease and a much bigger hypsochromic shift of the PL band (compared to irradiation at 492 nm). 280 nm wavelength light is strongly absorbed by both the Au NCs and the BSA coating. In this case photodegradation of Au NCs as well as of an Au NCs coating layer (BSA) can occur. Irradiation of the BSA solution with 280 nm light causes a decrease of the BSA PL band at 338 nm (data not shown). This indicates that the irradiation of BSA with 280 nm light causes photodegradation or conformational changes of BSA. Degradation of the Au NCs surface coating (BSA) makes Au NCs less protected from solvent (water) molecules and relaxation via surface defects can increase. This suggests that the degradation of BSA strongly influences the PL properties of BSA-Au NCs. The effect of

irradiation on the PL band at 468 nm was completely different when compared to the PL changes of the PL band at 660 nm. This leads to the suggestion that these two bands do not belong to the same material.

Under the irradiation of BSA-Au NCs with 280 nm light the PL intensity at 468 nm increased more than 5 times. We got very similar results when the pure BSA solution was irradiated with 280 nm light (Fig. 5(d)): the PL intensity at 468 nm increased more than 8 times during irradiation. This shows that the PL band at 468 nm is not related to the Au NCs PL but it corresponds to the phototransformation of BSA. Irradiation of the pure BSA solution under identical conditions causes a bigger increase in the PL intensity at 468 nm compared to the BSA-Au NCs solution. This can be explained in two ways: i) some of irradiation light is absorbed by Au NCs and does not induce any BSA damage; ii) the excited state of BSA can be quenched by Au NCs. Both of these processes reduce the phototransformation of BSA.

BSA does not absorb 405 nm light therefore phototransformation of BSA was not detected when the samples were irradiated using 405 nm light. However, 405 nm light is absorbed by BSA photoproducts and could be related to their photodegradation. This leads to a decrease of the PL intensity of the PL band at 468 nm. The irradiation at 492 nm does not induce any changes in the PL band at 468 nm because BSA and BSA photoproducts do not absorb light of this wavelength.

The irradiation of BSA-Au NCs in the Opti-MEM showed that the BSA-Au NCs exhibit greater photostability in this cell culture medium. The increased photostability of BSA-Au NCs in the Opti-MEM might be caused by the formation of an additional coating layer of BSA-Au NCs. The Opti-MEM medium contains proteins and amino acids. It was shown that proteins can increase the quantum yield and stability of nanoparticles [45] by the formation of "protein corona" around nanoparticles. The proteins can form a corona around BSA-Au NCs thus leading to better protection from the surrounding medium. It should be noted that the PL of BSA-Au NCs in the Opti-MEM at the same excitation conditions is slightly more intense than in a water solution (data not shown). This indicates that the quenching of BSA-Au-NCs PL in the Opti-MEM is lower than in water. This effect is probably achieved via the formation of an additional shielding layer – "protein corona".

5. Conclusions

We have shown that the synthesis of a BSA-Au nanocluster increases the hydrodynamic radius of BSA by 2.5 nm. The AFM measurement of BSA Au nanoclusters dispersed on the mica surface shows that the size of an Au nanocluster is less than 1.3 nm. This indicates that the size increase after the synthesis is caused by the conformation changes of BSA molecules induced by the formation of a gold nanocluster inside protein. BSA-Au nanoclusters exhibit great colloidal stability: their optical properties remain stable for more than 1 month (samples kept in the dark at 4 °C). BSA-Au nanoclusters do not degrade when heated up to 65 °C, yet they undergo some structural changes resulting in the decrease of PL intensity and a bathochromic PL band shift upon an increase in temperature. Nevertheless, these changes are reversible. These effects could be used for temperature sensing. Irradiation of BSA-Au nanoclusters causes big and irradiation wavelength dependent changes in the BSA-Au NCs PL spectra. Changes of the PL band at 660 nm caused by irradiation are similar under irradiation with 280, 405 and 492 nm light: the PL intensity decreases and the band shifts to the shorter wavelength region. However, the PL intensity decrease rate is higher when a shorter wavelength is used for irradiation. The effect of irradiation on the PL band at 468 nm was completely different when compared to PL changes of the PL band at 660 nm. The irradiation of BSA-Au NCs with 280 nm light increases PL intensity at 468 nm more than 5 times. Similar results are obtained when the pure BSA solution is irradiated with 280 nm light. This shows that the PL band at 468 nm corresponds to BSA photoproducts and is not related to the Au nanocluster formed inside BSA. We have also demonstrated that the cell growth medium Opti-MEM increases the photostability of BSA-Au nanoclusters. This effect is probably achieved via the formation of an additional shielding layer.

References

[1] J. Zheng, J.T. Petty, and R.M. Dickson, High quantum yield blue emission from water-soluble Au$_8$ nanodots, J. Am. Chem. Soc. **125**(26), 7780–7781 (2003), http://dx.doi.org/10.1021/ja035473v

[2] S.W. Chen, R.S. Ingram, M.J. Hostetler, J.J. Pietron, R.W. Murray, T.G. Schaaff, J.T. Khoury, M.M. Alvarez, and R.L. Whetten, Gold nanoelectrodes of varied size: transition to molecule-like

charging, Science **280**(5372), 2098–2101 (1998), http://dx.doi.org/10.1126/science.280.5372.2098

[3] S. Empedocles and M. Bawendi, Spectroscopy of single CdSe nanocrystallites, Acc. Chem. Res. **32**(5), 389–396 (1999), http://dx.doi.org/10.1021/ar9501939

[4] J.P. Xie, Y.G. Zheng, and J.Y. Ying, Protein-directed synthesis of highly fluorescent gold nanoclusters, J. Am. Chem. Soc. **131**(3), 888–889 (2009), http://dx.doi.org/10.1021/ja806804u

[5] H. Wei, Z.D. Wang, L.M. Yang, S.L. Tian, C.J. Hou, and Y. Lu, Lysozyme-stabilized gold fluorescent cluster: synthesis and application as Hg^{2+} sensor, Analyst **135**(6), 1406–1410 (2010), http://dx.doi.org/10.1039/C0AN00046A

[6] K. Chaudhari, P.L. Xavier, and T. Pradeep, Understanding the evolution of luminescent gold quantum clusters in protein templates, ACS Nano **5**(11), 8816–8827 (2011), http://dx.doi.org/10.1021/nn202901a

[7] E.S. Shibu, B. Radha, P.K. Verma, P. Bhyrappa, G.U. Kulkarni, S.K. Pal, and T. Pradeep, Functionalized Au_{22} clusters: synthesis, characterization and patterning, ACS Appl. Mater. Interfaces **1**(10), 2199–2210 (2009), http://dx.doi.org/10.1021/am900350r

[8] R.C. Jin, H.F. Qian, Z.K. Wu, Y. Zhu, M.Z. Zhu, A. Mohanty, and N. Garg, A methodology for synthesizing atomically precise gold nanoclusters, J. Phys. Chem. Lett. **1**(19), 2903–2910 (2010), http://dx.doi.org/10.1021/jz100944k

[9] Y.L. Xu, J. Sherwood, Y. Qin, D. Crowley, M. Bonizzoni, and Y.P. Bao, The role of protein characteristics in the formation and fluorescence of Au nanoclusters, Nanoscale **6**(3), 1515–1524 (2014), http://dx.doi.org/10.1039/C3NR06040C

[10] X. Yuan, Y. Yu, Q.F. Yao, Q.B. Zhang, and J.P. Xie, Fast synthesis of thiolated Au_{25} nanoclusters via protection-deprotection method, J. Phys. Chem. Lett. **3**(17), 2310–2314 (2012), http://dx.doi.org/10.1021/jz300960b

[11] Z.W. Wu, C. Gayathri, R.R. Gil, and R.C. Jin, Probing the structure and charge state of glutathione-capped $Au_{25}(SG)_{18}$ clusters by NMR and mass spectrometry, J. Am. Chem. Soc., **131**(18), 6535–6542 (2009), http://dx.doi.org/10.1021/ja900386s

[12] D.E. Jiang, M. Walter, and J. Akola, On the structure of a thiolated gold cluster: $Au_{44}(SR)_{28}^{2-}$, J. Phys. Chem. C **114**(38), 15883–15889 (2010), http://dx.doi.org/10.1021/jp9097342

[13] X.M. Wen, P. Yu, Y.R. Toh, and J. Tang, Structure-correlated dual fluorescent bands in BSA-protected Au_{25} nanoclusters, J. Phys. Chem. C **116**(21), 11830–11836 (2012), http://dx.doi.org/10.1021/jp303530h

[14] S.L. Raut, D. Shumilov, R. Chib, R. Rich, Z. Gryczynski, and I. Gryczynski, Two photon induced luminescence of BSA protected gold clusters, Chem. Phys. Lett. **561**, 74–76 (2013), http://dx.doi.org/10.1016/j.cplett.2013.01.028

[15] P. Yu, X.M. Wen, Y.R. Toh, and J. Tang, Temperature-dependent fluorescence in Au_{10} nanoclusters, J. Phys. Chem. C **116**(11), 6567–6571 (2012), http://dx.doi.org/10.1021/jp2120077

[16] S. Raut, R. Chib, R. Rich, D. Shumilov, Z. Gryczynski, and I. Gryczynski, Polarization properties of fluorescent BSA protected Au_{25} nanoclusters, Nanoscale **5**(8), 3441–3446 (2013), http://dx.doi.org/10.1039/C3NR34152F

[17] M. Matulionytė, R. Marcinonytė, and R. Rotomskis, Photoinduced spectral changes of photoluminescent gold nanoclusters, J. Biomed. Opt. **20**(5), 051018 (2015), http://dx.doi.org/10.1117/1.JBO.20.5.051018

[18] H. Kawasaki, H. Yamamoto, H. Fujimori, R. Arakawa, Y. Iwasaki, and M. Inada, Stability of the DMF-protected Au nanoclusters: photochemical, dispersion, and thermal properties, Langmuir **26**(8), 5926–5933 (2010), http://dx.doi.org/10.1021/la9038842

[19] H. Kawasaki, K. Yoshimura, K. Hamaguchi, and R. Arakawa, Trypsin-stabilized fluorescent gold nanocluster for sensitive and selective Hg^{2+} detection, Anal. Sci. **27**(6), 591–596 (2011), http://dx.doi.org/10.2116/analsci.27.591

[20] C.A.J. Lin, T.Y. Yang, C.H. Lee, S.H. Huang, R.A. Sperling, M. Zanella, J.K. Li, J.L. Shen, H.H. Wang, H.I. Yeh, W.J. Parak, and W.H. Chang, Characterization, and bioconjugation of fluorescent gold nanoclusters toward biological labeling applications, ACS Nano **3**(2), 395–401 (2009), http://dx.doi.org/10.1021/nn800632j

[21] Y.F. Kong, J. Chen, F. Gao, R. Brydson, B. Johnson, G. Heath, Y. Zhang, L. Wu, and D.J. Zhou, Near-infrared fluorescent ribonuclease-A-encapsulated gold nanoclusters: preparation, characterization, cancer targeting and imaging, Nanoscale **5**(3), 1009–1017 (2013), http://dx.doi.org/10.1039/C2NR32760K

[22] L.H. Jin, L. Shang, S.J. Guo, Y.X. Fang, D. Wen, L. Wang, J.Y. Yin, and S.J. Dong, Biomolecule-stabilized Au nanoclusters as a fluorescence probe for sensitive detection of glucose, Biosens. Bioelectron. **26**(5), 1965–1969 (2011), http://dx.doi.org/10.1016/j.bios.2010.08.019

[23] X.X. Wang, Y.Y. Wang, H.B. Rao, and Z. Shan, A sensitive fluorescent assay for trypsin activity in biological samples using BSA-Au nanoclusters, J. Brazil. Chem. Soc. **23**(11), 2011–2015 (2012), http://dx.doi.org/10.1590/S0103-50532012005000075

[24] H.W. Li, Y. Yue, T.Y. Liu, D.M. Li, and Y.Q. Wu, Fluorescence-enhanced sensing mechanism of BSA-protected small gold-nanoclusters to silver(I) ions in aqueous solutions, J. Phys. Chem. C **117**(31), 16159–16165 (2013), http://dx.doi.org/10.1021/jp403466b

[25] X. Wu, X.X. He, K.M. Wang, C. Xie, B. Zhou, and Z.H. Qing, Ultrasmall near-infrared gold nano-

clusters for tumor fluorescence imaging *in vivo*, Nanoscale **2**(10), 2244–2249 (2010), http://dx.doi.org/10.1039/c0nr00359j

[26] A. Retnakumari, S. Setua, D. Menon, P. Ravindran, H. Muhammed, T. Pradeep, S. Nair, and M. Koyakutty, Molecular-receptor-specific, non-toxic, near-infrared-emitting Au cluster-protein nanoconjugates for targeted cancer imaging, Nanotechnology **21**(5), 055103 (2010), http://dx.doi.org/10.1088/0957-4484/21/5/055103

[27] A.L. Zhang, Y. Tu, S.B. Qin, Y. Li, J.Y. Zhou, N. Chen, Q. Lu, and B.B. Zhang, Gold nanoclusters as contrast agents for fluorescent and X-ray dual-modality imaging, J. Colloid. Interf. Sci. **372**, 239–244 (2012), http://dx.doi.org/10.1016/j.jcis.2012.01.005

[28] G.Y. Sun, L. Zhou, Y.L. Liu, and Z.B. Zhao, Biocompatible Gd-III-functionalized fluorescent gold nanoclusters for optical and magnetic resonance imaging, New J. Chem. **37**(4), 1028–1035 (2013), http://dx.doi.org/10.1039/C3NJ00052D

[29] Z. Wu and R. Jin, On the ligand's role in the fluorescence of gold nanoclusters, Nano Lett. **10**(7), 2568–2573 (2010), http://dx.doi.org/10.1021/nl101225f

[30] X. Le Guevel, B. Hotzer, G. Jung, K. Hollemeyer, V. Trouillet, and M. Schneider, Formation of fluorescent metal (Au, Ag) nanoclusters capped in bovine serum albumin followed by fluorescence and spectroscopy, J. Phys. Chem. C **115**(22), 10955–10963 (2011), http://dx.doi.org/10.1021/jp111820b

[31] Y. Moriyama, D. Ohta, K. Hachiya, Y. Mitsui, and K. Takeda, Fluorescence behavior of tryptophan residues of bovine and human serum albumins in ionic surfactant solutions: A comparative study of the two and one tryptophan(s) of bovine and human albumins, J. Protein Chem. **15**(3), 265–272 (1996), http://dx.doi.org/10.1007/BF01887115

[32] S. Raut, R. Chib, S. Butler, J. Borejdo, Z. Gryczynski, and I. Gryczynski, Evidence of energy transfer from tryptophan to BSA/HSA protected gold nanoclusters, Methods Appl. Fluoresc. **2**(3) (2014), http://dx.doi.org/10.1088/2050-6120/2/3/035004

[33] R. Chib, S. Butler, S. Raut, S. Shah, J. Borejdo, Z. Gryczynski, and I. Gryczynski, Effect of quencher, denaturants, temperature and pH on the fluorescent properties of BSA protected gold nanoclusters, J. Lumin. **168**, 62–68 (2015), http://dx.doi.org/10.1016/j.jlumin.2015.07.030

[34] J.R. Lakowicz, *Principles of Fluorescence Spectroscopy*, 3rd ed. (Springer, Singapore, 2006) pp. 577–606, http://dx.doi.org/10.1007/978-0-387-46312-4

[35] A.K. Wright and M.R. Thompson, Hydrodynamic structure of bovine serum albumin determined by transient electric birefringence, Biophys. J. **15**, 137–141 (1975), http://dx.doi.org/10.1016/S0006-3495(75)85797-3

[36] J. Zheng, P.R. Nicovich, and R.M. Dickson, Highly fluorescent noble-metal quantum dots, Annu. Rev. Phys. Chem. **58**, 409–431 (2007), http://dx.doi.org/10.1146/annurev.physchem.58.032806.104546

[37] X.M. Wen, P. Yu, Y.R. Toh, A.C. Hsu, Y.C. Lee, and J. Tang, Fluorescence dynamics in BSA-protected Au$_{25}$ nanoclusters, J. Phys. Chem. C **116**(35), 19032–19038 (2012), http://dx.doi.org/10.1021/jp305902w

[38] B. Mali, A.I. Dragan, J. Karolin, and C.D. Geddes, Photophysical characterization and α-type delayed luminescence of rapidly prepared Au clusters, J. Phys. Chem. C **117**(32), 16650–16657 (2013), http://dx.doi.org/10.1021/jp4023184

[39] P.L. Xavier, K. Chaudhari, P.K. Verma, S.K. Pal, and T. Pradeep, Luminescent quantum clusters of gold in transferrin family protein, lactoferrin exhibiting FRET, Nanoscale **2**(12), 2769–2776 (2010), http://dx.doi.org/10.1039/C0NR00377H

[40] T. Das, P. Ghosh, M.S. Shanavas, A. Maity, S. Mondal, and P. Purkayastha, Protein-templated gold nanoclusters: size dependent inversion of fluorescence emission in the presence of molecular oxygen, Nanoscale **4**(19), 6018–6024 (2012), http://dx.doi.org/10.1039/C2NR31271A

[41] A.N. Kuznetsov, B. Ebert, G. Lassmann, and A.B. Shapiro, Adsorption of small molecules to bovine serum albumin studied by the spin-probe method, Biochim. Biophys. Acta **379**(1), 139–146 (1975), http://dx.doi.org/10.1016/0005-2795(75)90015-X

[42] V.J.C. Lin and J.L. Koenig, Raman studies of bovine serum albumin, Biopolymers **15**(1), 203–218 (1975), http://dx.doi.org/10.1002/bip.1976.360150114

[43] J. Oakes, Thermally denatured proteins. Nuclear magnetic resonance, binding isotherm and chemical modification studies of thermally denatured bovine serum albumin, J. Chem. Soc., Faraday Trans. 1, **72**, 228–237 (1976), http://dx.doi.org/10.1039/F19767200228

[44] R. Wetzel, M. Becker, J. Behlke, H. Billwitz, S. Böhm, B. Ebert, H. Hamann, J. Krumbiegel, and G. Lassmann, Temperature behaviour of human serum albumin, Eur. J. Biochem. **104**(2), 469–478 (1980), http://dx.doi.org/10.1111/j.1432-1033.1980.tb04449.x

[45] V. Poderys, M. Matulionyte, A. Selskis, and R. Rotomskis, Interaction of water-soluble CdTe quantum dots with bovine serum albumin, Nanoscale Res. Lett. **6**, 1–6 (2011), http://dx.doi.org/10.1007/s11671-010-9740-9

[46] W. Zhang, Y. Li, J. Niu, and Y. Chen, Photogeneration of reactive oxygen species on uncoated silver, gold, nickel, and silicon nanoparticles and their antibacterial effects, Langmuir **29**(15), 4647–4651 (2013), http://dx.doi.org/10.1021/la400500t

[47] M. Misawa and J. Takahashi, Generation of reactive oxygen species induced by gold nanoparticles

under x-ray and UV irradiations, Nanomedicine **7**(5), 604–614 (2011), http://dx.doi.org/10.1016/j.nano.2011.01.014

[48] H. Kawasaki, S. Kumar, G. Li, C.J. Zeng, D.R. Kauffman, J. Yoshimoto, Y. Iwasaki, and R.C. Jin, Generation of singlet oxygen by photoexcited $Au_{25}(SR)_{18}$ clusters, Chem. Mater. **26**(9), 2777–2788 (2014), http://dx.doi.org/10.1021/cm500260z

BALTYMU STABILIZUOTI AUKSO NANOKLASTERIAI: SPEKTRINIŲ SAVYBIŲ IR FOTOSTABILUMO TYRIMAI

V. Poderys [a], M. Matulionytė-Safinė [a, b], D. Rupšys [b], R. Rotomskis [a, b]

[a] *Nacionalinio vėžio instituto Biomedicininės fizikos laboratorija, Vilnius, Lietuva*
[b] *Lazerinių tyrimų centro Biofotonikos grupė, Vilnius, Lietuva*

Santrauka

Pastaruoju metu jaučio serumo albuminu stabilizuoti aukso nanoklasteriai (JSA-Au NK) sulaukė didelio susidomėjimo dėl galimo šių nanodalelių taikymo biomedicinoje. Šio tipo nanodalelės gali būti taikomos kaip fluorescenciniai ar daugiafunkciai žymenys, jutikliai, terapiniai agentai. JSA-Au nanoklasterių sintezė ir optinės savybės plačiai tiriamos, tačiau iki šiol literatūroje yra labai mažai duomenų apie šių nanodalelių fotostabilumą. Žinios apie švitinimo poveikį JSA-Au NK yra itin svarbios norint juos sėkmingai taikyti optinėje diagnostikoje ir terapijoje. Šviežiai susintetintas JSA-Au NK tirpalas turi dvi fotoliuminescencijos juostas: ties 468 ir 660 nm. JSA-Au NK pasižymi dideliu koloidiniu stabilumu, išlieka stabilūs juos kaitinant iki 65 °C. Mūsų atlikti tyrimai parodė, kad švitinant JSA-Au nanoklasterių tirpalą skirtingo bangos ilgio spinduliuote švitinimo poveikis fotoliuminescencijos juostoms ties 468 ir 660 nm yra skirtingas ir juosta ties 468 nm nepriklauso baltyme susidariusiam Au nanoklasteriui. Švitinant JSA-Au NK stebimas fotoliuminescencijos juostos ties 660 nm trumpabangis poslinkis. Šis efektas (tikriausiai susijęs su Au NK irimu) yra didesnis, kai švitinama trumpesnio bangos ilgio spinduliuote.